CrossMark

Strain-rate sensitivity of scratch hardness and deformation mechanism in nanocrystalline Ni under micro-scratch testing

Rongtao Zhu[1],*, Yanfeng Li[1], Xinxi Zhang[1], and Jianqiu Zhou[2]

[1] *School of Chemical Engineering and Technology, China University of Mining and Technology, Xuzhou 221116, China*
[2] *School of Mechanical and Power Engineering, Nanjing Technology University, Nanjing 210009, Jiangsu, China*

ABSTRACT

To investigate the strain-rate sensitivity in nanocrystalline (NC) materials using a single experimental technique over a wide range of strain rate, the micro-scratch testing technique was selected to obtain consistent and systematic data of the strain-rate sensitivity in a fully dense, high purity, and well-characterized electrodeposited NC Ni sample. The scratch characterizations and mechanical properties of the sample under the different scratch velocities were discussed in details. First, some critical parameters under the micro-scratch testing, such as strain rates, scratch ditch widths, were confirmed. Then, the scratch hardness under the different scratch velocity was investigated. From the results, the sample exhibits strain-rate sensitive mechanical properties. Further, the average values of strain-rate sensitivity of the sample were calculated. The values increase with increasing scratch velocity, and exhibit higher values that are of the order of 0.03–0.1. The greater strain-rate sensitivity exponents indicate that the NC Ni samples have different fundamental physical deformation mechanisms. Finally, the fundamental physical deformation mechanism under scratch testing was inspected using SEM and TEM technique. From the SEM and TEM morphologies, the grain boundary dislocation pile-ups should be a carrier of plastic flow under scratch testing in the NC Ni sample.

Introduction

NC materials, defined as polycrystalline materials with average grain size less than 100 nm, have attracted many studies currently due to their unusual mechanical and physical properties [1]. Wherein, there has been growing experimental evidence that NC materials exhibit highly strain-rate sensitive mechanical properties. For example, many NC metals strengthen with increasing of strain rate, and an increase in strain-rate sensitivity exponent occurs as the grain size decreases [2]. Lu et al. [3] investigated the effects of strain rate on the tensile flow of NC-electrodeposited Cu samples with an average

Address correspondence to E-mail: rtzhu2010@cumt.edu.cn

🙋 Springer

grain size of about 30 nm. They found that the flow stress was only mildly dependent on strain rate, and the flow stress at 1 % plastic strain increased from about 85 MPa to roughly 150 MPa within the strain rate range of 6×10^{-5}–1.8×10^{3} s^{-1}. Dalla Torre et al. [4] studied NC electrodeposited Ni with an average grain size of about 20 nm over a broad range of strain rates. The tensile strength was observed to be about 1500 MPa and constant for strain rates between 7×10^{-5} and 5.5×10^{-2} s^{-1}, but increased significantly for strain rates of 10–10^{3} s^{-1} to values as high as 2600 MPa, whereas Karimpoor et al. [5] observed that the flow stress of the fully dense NC-electrodeposited cobalt with a mean grain size of 12 nm exhibits strengthening behavior with the decreasing strain rate from 1×10^{-4} to 2.5×10^{-3} s^{-1}. Obviously, the experimental results about strain-rate sensitivity of strength in NC materials available in the literature are contradictory so far.

Moreover, the strain-rate sensitivity exponent of strength is a key parameter in evaluating the deformation mechanism of crystalline materials. Different strain-rate sensitivity exponents indicate that crystalline materials have different fundamental physical deformation mechanisms from conventional coarse-grained metals to their NC counterparts. Especially, different regions of mechanical behaviors naturally develop within broad ranges of strain rates for NC metals. To examine how the strain-rate sensitivity exponent of strength changes with the operate deformation mechanism for NC materials, Humphrey et al. [6] systematically investigated the strain-rate sensitivity of strength in macro-to-micro-to-nano-crystalline Ni, and found that the strain rate sensitivity exponents vary with the stain rate and grain size. When strain rate $\dot{\varepsilon} < 10^{-3}$s^{-1}, strengthening of crystalline Ni is attributed to solution chemistry or alloy content, and the strain-rate sensitivities of NC and microcrystalline Ni samples are very small. In second region (10^{-3}s$^{-1} < \dot{\varepsilon} < 10^{3}$s^{-1}), the additional effect of dislocation activity adds to the strengthening response and the strain-rate sensitivity of NC metal is greater than that of microcrystalline FCC metal. Into range of 10^{3}s$^{-1} < \dot{\varepsilon}$), the NC metal Ni exhibits a singular strength value due to lager lattice distortions that affect the mobility of dislocations through the lattice. Jia et al. [7] studied the mechanical behaviors of consolidated iron with average grain sizes from tens of nanometers to tens of microns systematically

under uniaxial compression over a wide range of strain rates. They indicated that the NC Fe exhibits diminished effective strain-rate sensitivity of the flow stress due to the change of deformation mode from uniform deformation to shear localization in NC Fe under high strain rate. The same trend was also predicted by theoretical modeling [8] and experimental observation [9]. Cheng et al. [10] reported the mechanical properties of the NC Cu prepared by ball milling and consolidation technique, and demonstrate an elevated strain-rate sensitivity of flow stress in the NC Cu samples and explain this behavior in term of the thermally activated deformation mechanisms under quasi-static strain rate. However, Zhu et al. [11] and Chan et al. [12] considered that the strengthening of NC Ni with increasing strain rate can be attributed to the strain localization in form of shear bands under quasi-static tensile loads.

As mentioned above, many of the experimental results available in the literatures on strain-rate sensitivity of NC metals cannot easily be compared. Especially, some data about change trend of strain-rate sensitivity in NC metals are contradictory. There may be several factors that cause the phenomenon. One is produce techniques of NC metals, the different produce techniques usually results in widely different internal structures and processing-induced artifacts. These differences render it difficult to confirm the mechanisms responsible for differences in mechanical properties. Another, different specimen designs, loading method, displacement and strain monitoring technique, and precision of data are involved in experiments at different strain rates generally. For instance, the experimental results obtained from quasi-static strain rate tests were directly made a comparison with the experimental data from high strain rate tests. Further, different sized samples are used when different instruments, test techniques, and loading methods are utilized, which may influence the mechanical response.

Therefore, the quantitative experimental results available in the literatures on the strain-rate sensitivity of NC metals are not conclusive and different deformation mechanisms of the NC metals at different ranges of strain rate are not well understood so far, since the deformation mechanism will vary with the increasing strain rate. So it is a critical need to use a single experimental technique to obtain consistent and systematic data of the strain-rate sensitivity of NC metals over a wide range of strain rate in a fully dense, high purity, and well-characterized sample.

Yoo et al. [13] studied the effect of grain size on dynamic compression properties of NC tantalum consolidated by plasma pressure compaction, and Zhu et al. [14] investigated the impact mechanical properties of NC Ni prepared by high energy ball milling using Split Hopkinson Bar testing under high strain rate, but the experimental data obtained under this testing technique usually exhibit a phenomenon of vibration due to dispersion effect of dynamic impact, which may affect the precision of experimental data. Thus, micro-scratch testing technique is a preferable method, since the technique can provide consistent and systematic data of scratch hardness over a wide range strain rate for the same sample vary with depth of scratch groove.

Experiment procedure

Sample preparation

Commercially available electrodeposited NC Ni was selected to study the mechanical properties of NC metals, larger dimension (i.e., $76.2 \times 76.2 \times 0.2$ mm^3 thick), fully dense electrodeposited NC Ni sheets with a purity of 99.9 % were purchased from Integran Technologies Inc. (Canada). First, the sheets were polished on one side using SiC paper with diamond suspensions of 3, 1, and 0.25 μm grain size, respectively. After the polishing procedure, the thickness of the sheet reaches to 150 μm. Then, rectangular samples (25×15 mm^2) for micro-scratch testing were electro-discharge machined from the polished NC Ni sheets, and the rectangular samples were glued onto a toughened glass bulk using a standard cyanoacrylate glue. The samples were put aside for at least 24 h after gluing onto the glasses, and then the micro-scratch tests were performed. For comparison, dog-bone-shaped samples for tensile test were also electro-discharge machined from the polished NC Ni sheets. The width and length of the tensile sample gage section were 10 and 30 mm, respectively and thickness is, approximately 150 μm. These tensile samples have centimeters in gage section that allow conventional tensile tests.

Tensile and micro-scratch testing

Tensile tests were carried out at room temperature with Zwick BZ2.5/TS1S universal test machine at fixed quasi-static strain rates, ranging from 5×10^{-3} to 5×10^{-1} s^{-1} (displacement control mode). The test machine has a specially designed fixture that possesses an immovable bottom grip and a moving upper grip, both of which were supported by pivots to minimize bending in the sample. Meanwhile, strain measurements were confirmed by measuring the elongations in the gage length.

Micro-scratch tests were performed using a CSM Instruments model Micro-Combi Tester at about 20 °C and 40 % RH. Spherical Rockwell W-209 diamond indenter, 200 μm tip radius, was chosen as blunt micro-contact geometry. In this experiment, the micro-scratch tests were split into three steps. First, the indenter measured the starting surface profile with a very small and constant load of 1 N, along the scratch pattern; this step can be called pre-scan; then the indenter returned to the starting location to perform the scratch with a progressive loading (loaded scratch scan) along the same pattern; finally the indenter went back to the starting location again after the loaded scratch scan to measure the profile of the scratch groove with a small and constant load (1 N); this step was marked as post-scan. During the test, normal forces under the progressive loading were on-line monitored using a real-time force feedback transducer, and the progressive load scratch test was performed by using an overall scratch length of 2 mm and scratch speeds of 0.6, 6, 30, 80, and 150 mm/min, respectively. To ensure the depth of scratch groove does not exceed the radius of indenter tip, a peak of the progressive loading program should be less than 30 N in this experiment.

From the scratch testing, the depth of surface penetration can be calculated by subtracting the starting surface profile measured during pre-scan from the scratch profile measured during the loaded scratch scan. Meanwhile, residual deformation response was estimated by using the post-scanned profile of the scratch pattern; the residual scratch ditch could be usefully confirmed by subtracting the extent of immediate recovery of scratch groove from the depth of surface penetration. The widths of the residual scratch groove with the increasing load can be measured using digital enhancement of optical microscopy conducted at 40× magnification.

Moreover, each scratch test was replicated, at least, three times in this experiment and the minimum distance between scratches was kept above 3 mm. In this way, the results could be considered

representative of the average response over greater surfaces of the NC Ni sample area.

Characterization for micro-scratch testing

To inspect the fracture mode and deformation mechanisms of NC Ni sheet under the micro-scratch testing, the zones around the scratch ditch tip were characterized using SEM and TEM methods. Schematic for SEM and TEM samples preparation after the micro-scratch testing is shown in Fig. 1. For SEM observations, the sheets were broke along the centerline of the scratch ditch to investigate the surface morphology of the scratch ditch tip (Fig. 1a). The SEM observation was operated with a JEOL 6400 FESEM operating at 20 kV. Moreover, a disks sample with diameter of 3 mm for TEM investigation was also extracted from the zone of scratch ditch tip, as shown in Fig. 1b. First, the disks were polished on the bottom side (opposite the top side with scratch ditch) to thin by about 60 μm, Then, the sample was twin-jet polished again in an electrolytic bath of 10 % perchloric acid and 90 % ethanol at −10 °C and 50 V. Finally, the thin disks sample was put in a JEM-200CX TEM operating at 300 kV to observe the microstructure morphology.

Results and discussion

Microstructure of NC Ni sheet

Figure 2a shows the representative TEM bright field image together with the corresponding selected area diffraction (SAD) patterns of the grain morphology

(inset of the Fig. 2a) of the NC Ni sheet. From the TEM morphology, the shapes of the grains are mainly equiaxed. Meanwhile, the SAD patterns with indexing of the rings are shown in Fig. 2b, and the results of indexing of the rings are given in Table 1. It is clearly that interplanar distances measured from the corresponding diffraction rings have a good agreement with standard ones of pure fcc Ni, suggesting that no second phase is present in electrodeposited NC Ni sheet.

Mechanical behaviors under tensile and micro-scratch testing

Theoretical model

The strain-rate sensitivity of strength provides information about the mode of deformation as seen in the onset of plasticity or the initiation of a flow stress. In general, the value of strain–rate sensitivity for strength is determined from the slope to a linear fit for the log–log scale plot of flow stress (σ) versus strain rate (ε) under tensile testing, it can be written as

$$m = \partial \left(\ln \sigma\right)/\partial \left(\ln \dot{\varepsilon}\right). \tag{1}$$

For the micro-scratch test method [15, 16], the scratch hardness (H_s) should be substituted into the equation above in place of the strength to determine strain-rate sensitivity exponent as
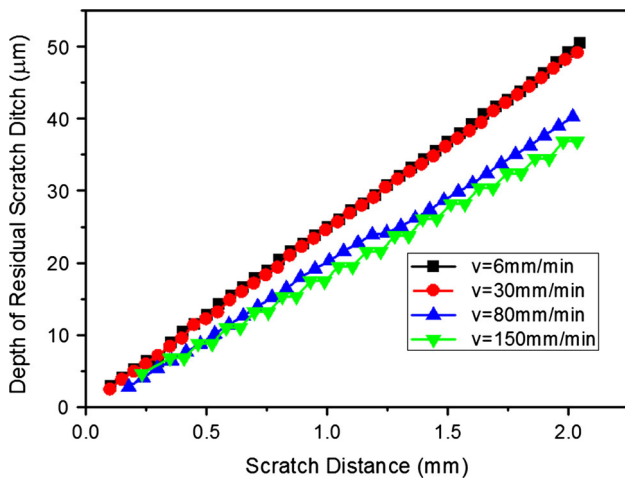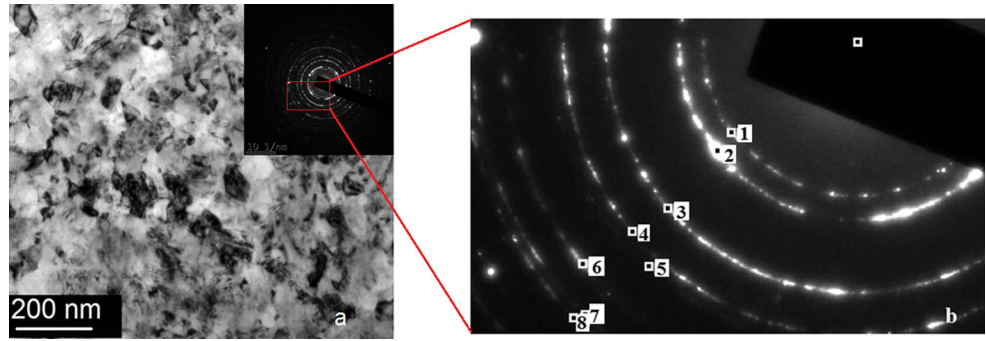
$$m = \partial \left(\ln H_s\right)/\partial \left(\ln \dot{\varepsilon}\right). \tag{2}$$

where the scratch hardness can be determined by the expression for scratch hardness as a function of the scratch width (w) and the indent load (N), it is given as

Figure 1 Schematic for SEM (**a**) and TEM (**b**) sample preparation around the scratch ditch tip after the micro-scratch testing for the NC Ni sheet.
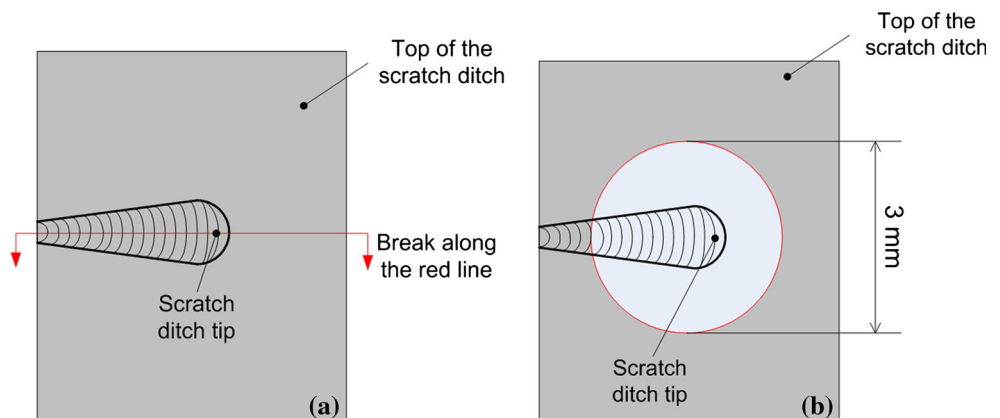
Figure 2 **a** TEM bright field micrograph accompanying the corresponding SAD pattern of the grain morphology of commercially available electrodeposited NC Ni, **b** the SAD patters with indexing of the rings.

Figure 3 The depths of residual scratch ditch varying with the scratch distance at different micro-scratch speeds.

$$H_s = k \cdot N / w^2. \qquad (3)$$

Here the parameter k is a geometric constant that is specific to the indenter tip shape. If the indentation scratch does not extend beyond the radius of indenter tip, then the parameter k equals $8/\pi$. The value is derived for a projection of the leading half of the hemispherical tip. So, the scratch loads in our experiments are selected to produce scratches that do not extend in width beyond an equivalent to the

hemispherical projection of the indenter tip. Meanwhile, an empirical formula [17] for strain rate ($\dot{\varepsilon}$) as a function of micro-scratch velocity (v) and the width of scratch groove (w) is given as

$$\dot{\varepsilon} = C \frac{v}{w} \qquad (4)$$

Here C is a constant expressing the effective strain (ε_s) and introduced to account for the relative strain imposed due to the indenter geometry. In particular, for a spherical blunt contact, the effective strain ε_s could be considered proportional to the relative strain r/R', where r is the radius of the efficient contact between the indenter and the sample surface and R' is the radius of the spherical geometry at the end of the scratch tip. From this equation, the decreasing strain rate with the progressive normal force at each constant micro-scratch velocity can be calculated, since the width of scratch groove increases with the increasing normal force. Thus, the slope of the log–log scale variation of strain rate versus scratch hardness can be used to measure the strain-rate sensitivity exponent.

Scratch characterization and mechanical behaviors

Figure 3 gives the trend of the depths of residual scratch ditch varying with the scratch distance at

Table 1 Results of indexing of SAD patterns for electrodeposited NC Ni sheet and comparison of interplanar distances between NC Ni and standard pure Ni

Number of rings		1	2	3	4	5	6	7
Crystal face		(111)	(200)	(220)	(311)	(222)	(400)	(331)
Interplanar distance	NC Ni	0.2025	0.1771	0.1245	0.1067	0.1025	0.0889	0.0815
	Standard pure Ni	0.2041	0.1768	0.1250	0.1066	0.1020	0.0884	0.0811
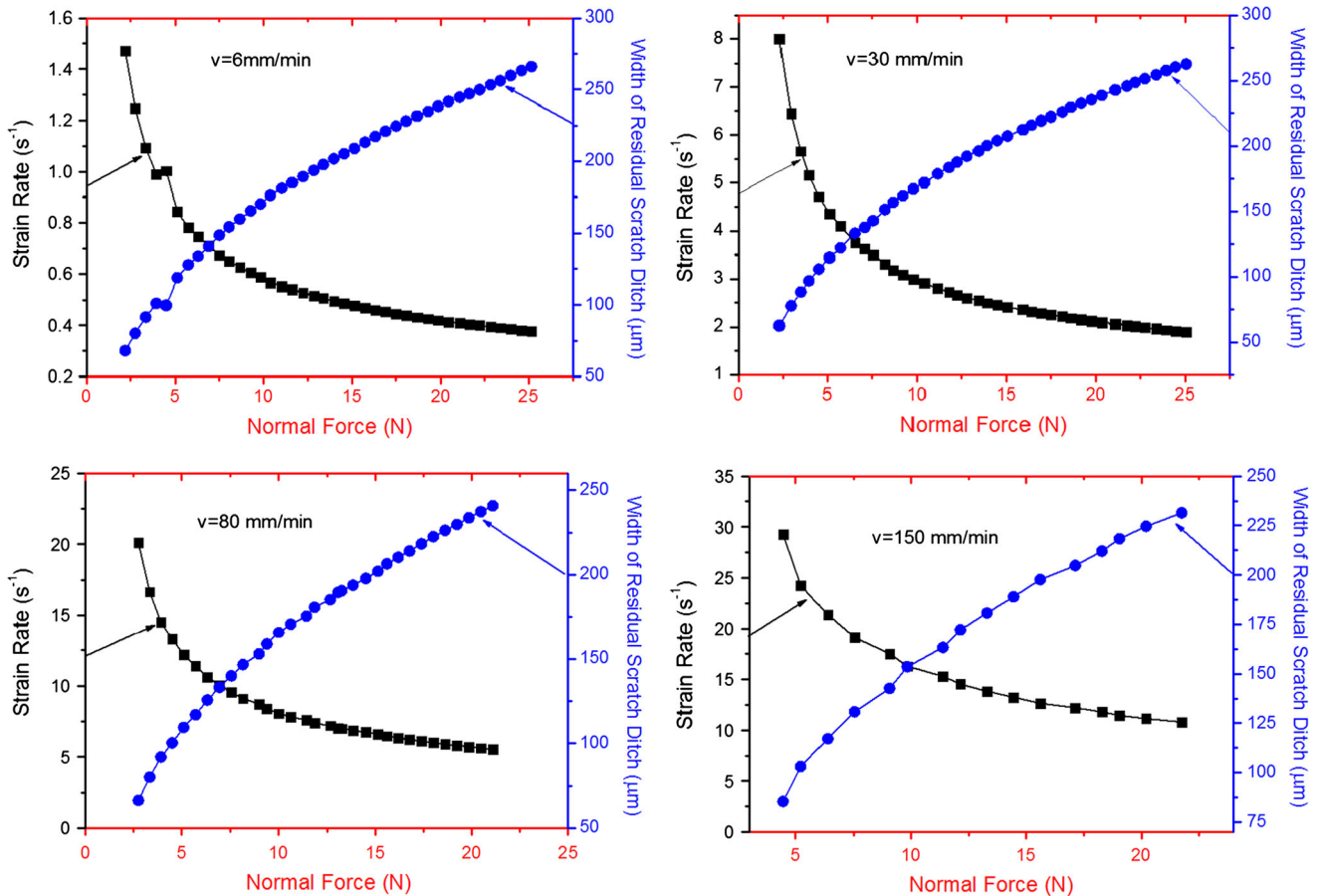
Figure 4 The widths of residual scratch ditch and strain-rate with the increasing normal force for each scratch velocity during the scratch testing.
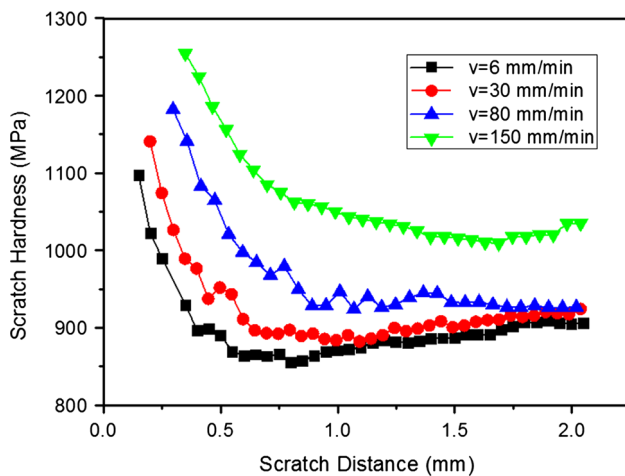

Figure 5 The scratch hardness as a function of scratch distance under the different scratch velocities.

different micro-scratch velocities during the scratch testing. To eliminate the effect of elastic deformation of the sample, the depth of residual scratch ditch under the progressive loading was confirmed by subtracting the extent of immediate recovery of scratch ditch from the depth of surface penetration after post-scan. From Fig. 3, the maximum of the residual depth of scratch grooves is about 50 μm that does not exceed the radius of the scratch indenter. Meanwhile, the depths of residual scratch ditch under each micro-scratch speed increase with the increasing scratch distance from 0 to 2 mm, and curves of the depth become disperse at larger scratch distance stage. However, the residual depths of the scratch grooves weaken gradually with the increasing micro-scratch velocity, though the value at very close quarters under scratch velocities of 6 and 30 mm/min. According to the depth of residual scratch ditch, the radius r of the efficient contact between the indenter and the sample surface can be determined through the equation as

$$r = \sqrt{R^2 - (R - d_R)^2}. \tag{5}$$
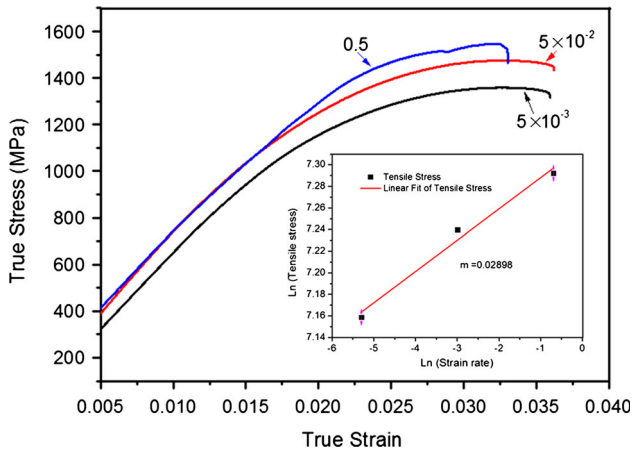
Figure 6 True tensile stress–strain curves for the NC Ni samples at strain rate of 5×10^{-1}, 5×10^{-2}, and 5×10^{-3} s^{-1}. *Inset* of the figure shows that Ln–ln plot between tensile stress and strain rate and the strain rate sensitivity for tensile testing under quasi-static strain rate is about 0.02898 by fitting.
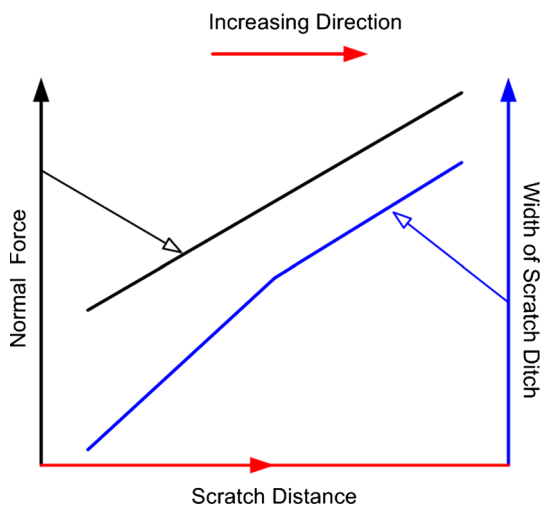
Figure 7 Schematic for the width of scratch ditch and normal force varying with scratch distance under scratch testing.

Here R is the radius of scratch indenter and d_R is the depth of residual scratch ditch. Therefore, continuous changing strain-rates under each scratch velocity can be confirmed through Eq. (4), since the widths of the residual scratch groove with the increasing load can be measured using digital enhancement of optical microscopy.

Figure 4 reports the width of residual scratch ditch measured by optical microscopy and strain-rate calculated by Eq. (4) with the increasing normal force for each scratch velocity during the scratch testing. Obviously, the residual scratch ditches widen

gradually for each scratch velocity with the increasing normal force under scratch testing, and the width of residual scratch ditch becomes small under larger scratch velocity. For example, the value of the width is about 275 μm at the end of normal force or scratch distance under velocity of 6 and 30 mm/min; the value is about 250 and 230 μm respectively for the scratch velocity of 80 and 150 mm/min. At the same time, the strain rate under the scratch test for each scratch velocity decreases with increasing normal force or scratch distance due to the widening of residual scratch ditch according to the Eq. (4). From Fig. 4, the strain rate covers a range from 0.3 to 30 s^{-1} approximately when the scratch velocity increases from 6 to 150 mm/min.

Figure 5 shows the scratch hardness calculated by Eq. (3) as a function of scratch distance under the scratch velocity of 6, 30, 80, and 150 mm/min, respectively. From the figure, the scratch hardness exhibits a rate-dependence behavior, and becomes stronger at larger scratch velocity. The maximal values for the NC Ni sample are 1254 MPa at a scratch velocity of 150 mm/min; 1182 MPa at a scratch velocity of 80 mm/min; 1141 MPa at a scratch velocity of 30 mm/min and 1097 MPa at a scratch velocity of 6 mm/min. A similar tendency is found for NC tensile samples; as shown in Fig. 6, the tensile stress–strain curves also exhibit rate-dependent strength, and the flow strengths increase as growing strain rate. Moreover, the values of yield strength of the tensile samples, determined using the intercept of the stress–strain curves with the 0.2 % total strain offset parallel to the elastic slope, are about 1081 MPa, 1157 MPa, and 1182 MPa under the strain rate of 5×10^{-3}, 5×10^{-2}, and 5×10^{-1} s^{-1}, respectively. It is clear that the yield strengths under tensile testing can roughly match with the maximal scratch hardness values at beginning of scratch ditch under different scratch velocities.

Meanwhile, from Fig. 5 the scratch hardness values progressively strengthen as the scratch distance decreases for each scratch velocity when the scratch distance is less than 1 mm. As shown in Fig. 4, the inverse proportion was exhibited between strain rate and scratch distance under progressive loading, so the scratch hardness values gradually increase with the increasing strain rate for each scratch velocity over the range of distance from 0 to 1 mm. However, the increasing trend of scratch hardness as the scratch velocity increases is inconspicuous over a range of
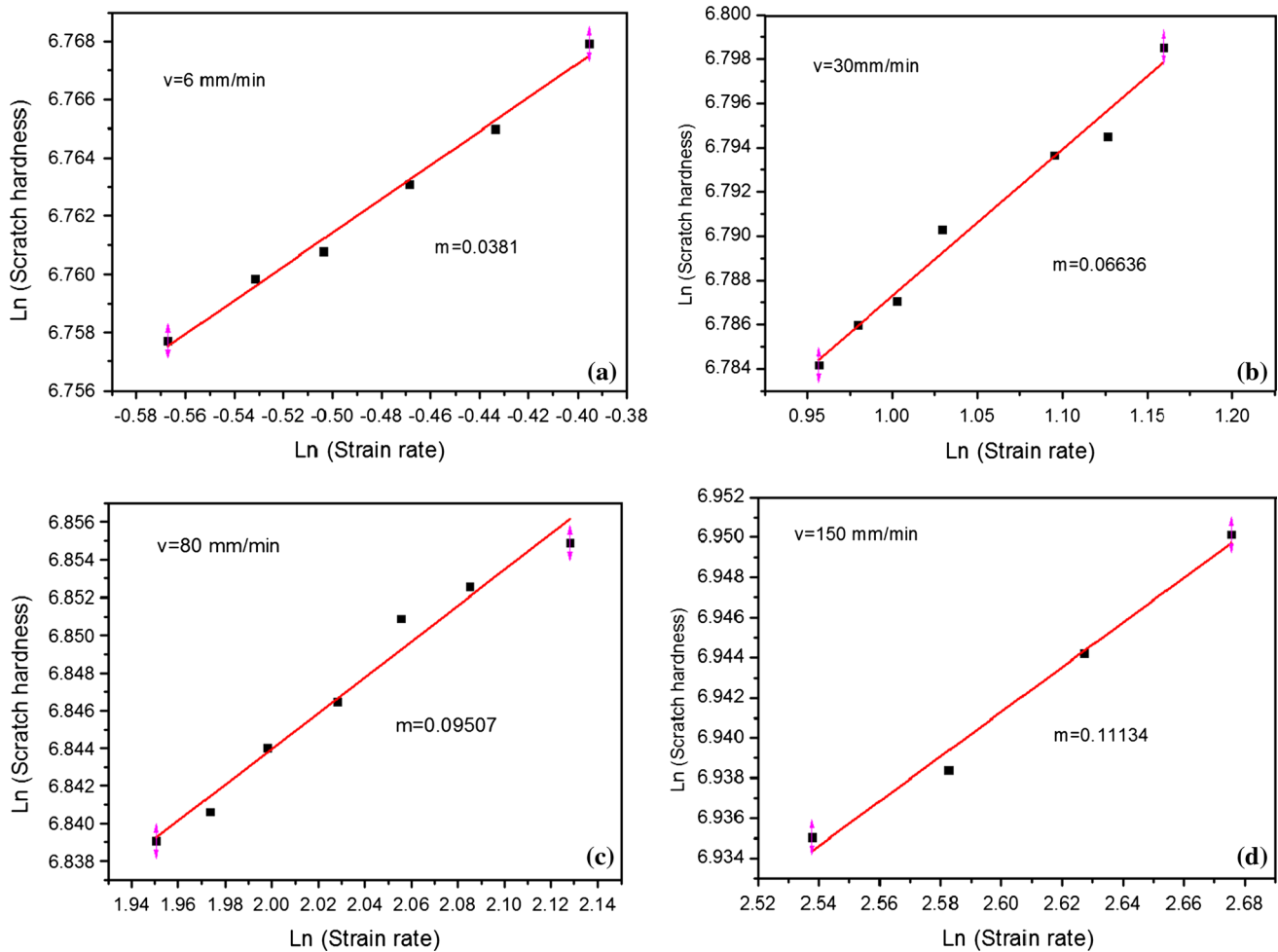
Figure 8 Ln–ln plot showing the relationships between scratch hardness and strain rate for different scratch velocities, over the range of smaller scratch distance.

scratch distance from 1 to 2 mm, except the value at scratch velocity of 150 mm/min. At the same time, the scratch hardness values nearly keep constant for each scratch velocity over the range of scratch distance from 1 to 2 mm. In other words, there is no rate-dependent behavior of scratch hardness over the distance range for single scratch velocity, although the strain rate also increases as the scratch distance reduces at the range. We considered that the behavior over the range of the larger scratch distance can not reflect the intrinsic character of the NC Ni sample due to plastic pile-ups formed on two edges and front of scratch ditch under larger scratch distance (normal force) during the micro-scratch testing, the plastic pile-ups can be seen in SEM morphology in Fig. 9. To explain the effect of the plastic pile-ups on the mechanical behavior of NC Ni sample, a schematic

for the width of scratch ditch and normal force varying with scratch distance was plotted in Fig. 7. The growth rate of scratch ditch width exhibits different values over the two ranges of scratch distance, and the value over the range of larger scratch distance is smaller due to plastic pile-ups, while the increase rate of normal force is constant for each scratch velocity. Therefore, the variation of scratch hardness over larger scratch distance is unapparent because the increase rate between normal force and scratch ditch width is equivalent. In contrast, there is no or very slight effect of plastic pile-ups on the width of scratch ditch at smaller scratch distances, so the growth rate of scratch ditch width is higher, and the scratch hardness obviously increases for each scratch velocity as the scratch distance reduces.
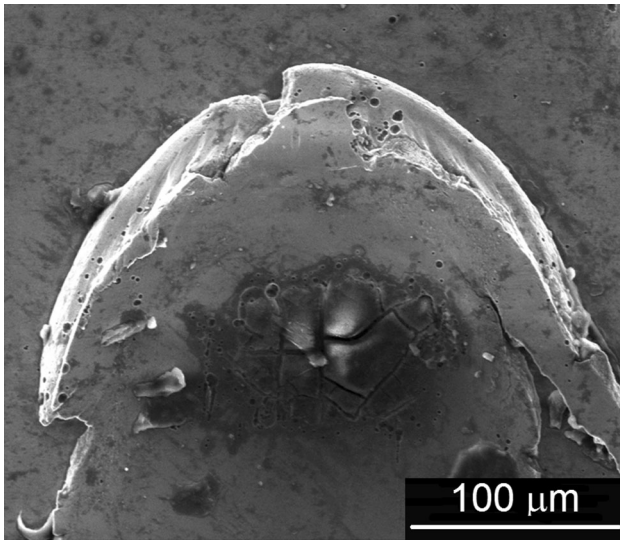
Figure 9 SEM morphology of whole scratch ditch tip for NC Ni sample under the scratch velocity of 6 mm/min.
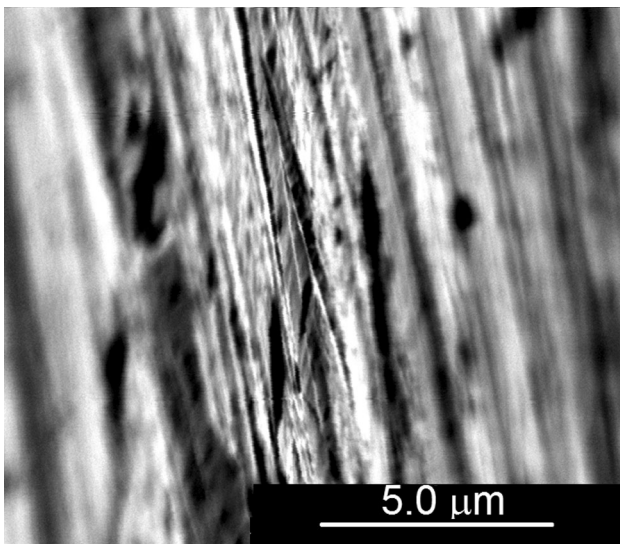
Figure 10 The lateral SEM morphology of the scratch ditch tip under the scratch velocity of 6 mm/min.

Strain-rate sensitivity of NC Ni under scratch testing

From "Scratch characterization and mechanical behaviors" section, the mechanical behaviors of the NC Ni sample were significantly influenced by plastic pile-ups over the range of larger scratch distance. So the values of scratch hardness over the range are introduced with larger errors under micro-scratch testing. To try to ensure accuracy of data during the scratch testing, the values of scratch hardness for each scratch velocity over the range of smaller scratch distance (less than 1 mm) were selected to investigate the strain-rate sensitivity exponent under the scratch testing. Figure 8 shows the relationships between scratch hardness and strain rate for scratch velocities of 6, 30, 80, and 150 mm/min respectively in a logarithm format according to the mechanical responses over the range of smaller scratch distance. From these figures, the values of the strain-rate sensitivity under different scratch velocities can be obtained from the slope of the log–log scale variation of strain rate versus scratch hardness using linear fitting method, the results were listed in the figures and the values are 0.0381, 0.06636, 0.09507, and 0.11134 under the scratch velocities of 6, 30, 80, 150 mm/min, respectively. Obviously, the values of strain-rate sensitivity increase with increasing scratch velocity, and the values under the four different scratch velocities (the strain rate varies from 0.37 to 30 s^{-1} approximately) are greater than the value of tensile sample as shown in the inset of Fig. 6 ($m = 0.02898$), whereas the strain rate sensitivity exponent obtained from small scratch velocity, i.e., 6 mm/min, is comparable to that from the tensile testing. This successive change of strain rate sensitivity indicates that the scratch technique is feasible to assess the rate sensitivity exponent of NC metals under higher strain rates. Compared with the value from the tensile testing, the greater strain-rate sensitivity under scratch testing suggests that the plastic flow mechanisms in NC Ni sample are different with the plastic flow mechanisms of their conventional coarse-grained counterparts. The underlying deformation mechanisms in the NC Ni sample under scratch testing will be discussed in details in the following section.

Deformation mechanism of NC Ni under scratch testing

It is well known that for coarse-grained fcc metals the transgranular dislocation-mediated deformation mechanism is responsible for the plastic flow, and the rate–dependent of this mechanism is not obvious; for example, the strain rate sensitivity exponent of conventional coarse-grained Cu is about 0.006 [10]. On the contrary, the plastic deformation of NC metals, especially for the metals with tiny grain size ($d < 20$ nm), is mainly controlled by grain boundary mediated mechanism [18, 19], such as grain boundary sliding, this grain boundary mediated mechanism
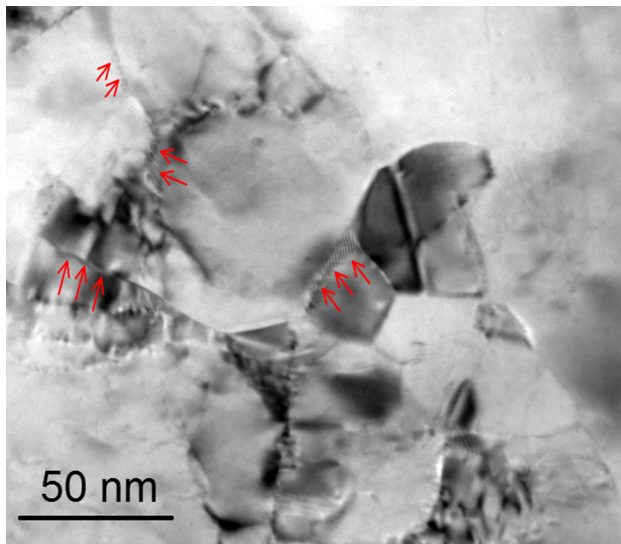
Figure 11 TEM morphology of the scratch ditch tip for NC Ni sample at the scratch velocity of 6 mm/min. It is clear that the dislocations accumulate at grain boundaries.
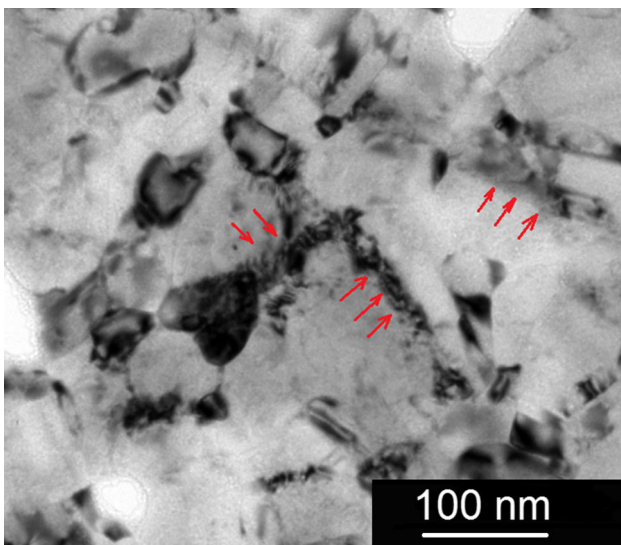
Figure 12 TEM morphology with grain elongation (marked by *red arrows*) for the scratch ditch tip under the scratch velocity of 6 mm/min.

usually exhibits higher value of strain-rate sensitivity that may be of the order of 0.5–1. Therefore, the strain-rate sensitivity exponent of scratch hardness can provide some information about the deformation mode and deformation mechanism. It is clear that the strain-rate sensitivity of the NC Ni sample under scratch testing in our experiment is greater than that of conventional metals, but lower than that of NC

metals with tiny grain size. So we consider that a special deformation mechanism that is different with the mechanisms in conventional and tiny grained metals should be a carrier of plastic flow in bulk NC Ni samples under the scratch testing.

To study the deformation mechanism of NC Ni sample under scratch testing, the zones around the scratch ditch tip were selected for SEM and TEM investigation. The preparation procedures of SEM and TEM specimens were shown in "Characterization for micro-scratch testing" section. First, the whole morphology of the scratch ditch tip for the scratch velocity of 6 mm/min investigated by SEM is presented in Fig. 9. From the figure, the NC Ni sample shows a brittle intergranular fracture mode; the crystal grains seem to be torn along the grain boundaries. Meanwhile, Fig. 10 shows the lateral morphology of the scratch ditch tip under the same condition using SEM technique. Obviously, representative brittle fracture surface with some glide bands can be observed, though blurry zones at the two sides of the picture occur due to the unevenness of the scratch ditch.

To further inspect the underlying mechanism caused the fracture mode, the TEM morphologies of the scratch ditch tip under the scratch velocity of 6 mm/min are shown in Fig. 11. Clearly, several grain boundary dislocations (marked by red arrows) are found in the TEM morphology. So, the brittle mode of fracture surface should be attributed to the accumulation of dislocation at grain boundaries, and this kind of grain boundary dislocation is different with the transgranular dislocations in coarse-grained metals. In NC metals, the volume fraction of grain boundary increases significantly with the decreasing grain size [20]; the fraction can reach 50 % when the grain size is about 10 nm. So the grain boundaries have a significant role during the deformation process of NC metals. In NC Ni sample under the scratch testing, the dislocations first nucleate at grain boundaries accordingly and then grow gradually with the increasing normal force or scratch distance under the scratch testing in this paper. On the one hand, with the increasing of scratch velocity, dislocations accumulate at grain boundaries more and more quickly and dislocation density increases rapidly for the higher scratch velocity, so the NC Ni sample presents larger scratch hardness under higher scratch velocity, as shown in Fig. 5. On other hand, the accumulation of the grain boundary dislocations

causes the distortion of grain lattice and drives the sliding of grain boundaries proved by elongation of grain in the NC Ni sample, as shown in Fig. 12. Conversely, the grain elongation can certify the activity of grain boundary dislocation in the NC Ni sample. Finally, the grain boundary sliding and distortion of grains driven by the grain boundary dislocation trigger the failure of the sample along the grain boundaries, and intergranular cracks form during the scratch testing. Therefore, the NC Ni sample exhibits a brittle intergranular fracture mode. According to the SEM and TEM morphologies, the grain boundary dislocation mechanism should be dominant during the plastic flow of NC Ni sample under scratch testing.

Conclusion

The strain-rate sensitivity exponent of strength is a key parameter in evaluating the deformation of NC metals. To investigate the strain-rate sensitivity in NC materials, the micro-scratch testing technique was chosen as a preferable method to provide consistent and systematic data of the strain-rate sensitivity over a wide range of strain rate in a fully dense, high purity and well-characterized electrodeposited NC Ni sample, and scratch characterizations and mechanical properties of the NC Ni sample under the different scratch velocities were discussed in details. First, the strain rates varying with scratch distance were investigated. It is clear that the strain rate covers a range from 0.3 to 30 s^{-1} approximately as the scratch velocity increases from 6 to 150 mm/min in our experiment. Second, the scratch hardness under different scratch velocities was discussed. From the experimental results, the scratch hardness exhibits a rate-dependence behavior and shows strengthening response with increasing scratch velocity. The maximal value at a scratch velocity of 150 mm/min for the NC Ni sample is 1254 MPa. Meanwhile, the scratch hardness values progressively strengthen as the scratch distance decreases for each scratch velocity when the scratch distance is less than 1 mm, while the scratch hardness values nearly keep constant for each scratch velocity over the range of scratch distance from 1 to 2 mm due to plastic pile-ups formed on two edges and front of scratch ditch during the micro-scratch testing. Further, the values of strain-rate sensitivity of the NC Ni sample under different scratch velocities were derived from the slopes of the log–log scale variation of strain rate versus scratch hardness. The values are 0.011134 at a scratch velocity of 150 mm/min; 0.09507 at a scratch velocity of 80 mm/min; 0.06636 at a scratch velocity of 30 mm/min; and 0.0381 at a scratch velocity of 6 mm/min. Obviously, the value of strain-rate sensitivity under the four different scratch velocities is much greater than the value of conventional coarse-grained fcc metals. The greater strain-rate sensitivity exponents indicate that the NC Ni samples have different fundamental physical deformation mechanisms compared with conventional coarse-grained counterparts. Finally, the fundamental physical deformation mechanism of NC Ni sample under scratch testing was inspected using SEM and TEM technique for the scratch ditch tip. The dislocations were accumulated in grain boundaries, and the grain boundary dislocation pile-ups should be a carrier of plastic flow under scratch testing in the NC Ni sample.

Compliance with ethical standards

Conflict of interest The authors declare that they have no conflict of interest.

References

[1] Meyers MA, Mishr AA, Benson DJ (2006) Mechanical properties of nanocrystalline materials. Prog Mater Sci 51:427–557

[2] Schwaiger R, Moser B, Dao M, Chollacoop N, Suresh S (2003) Some critical experiments on the strain-rate sensitivity of nanocrystalline nickel. Acta Mater 51:5159–5172

[3] Lu L, Li SX, Lu K (2001) An abnormal strain rate effect on tensile behavior in nanocrystalline copper. Scripta Mater 45:1163–1169

[4] Dalla Torre F, Van Swygenhoven H, Victoria M (2002) Nanocrystalline electrodeposited Ni: microstructure and tensile properties. Acta Mater 50:3957–3970

[5] Karimpoor AA, Erb U, Aust KT, Palumbo G (2003) High strength nanocrystalline cobalt with high tensile ductility. Scripta Mater 49:651–656

[6] Humphrey RT, Jankowski AF (2011) Strain-rate sensitivity of strength in macro-to-micro-to-nano crystalline nickel. Surf Coat Tech 206:1845–1849

[7] Jia D, Ramesh KT, Ma E (2003) Effect of nanocrystalline and ultrafine grain sizes on constitutive behaviors and shear bands in iron. Acta Mater 51:3495–3509

[8] Zhou JQ, Zhu RT, Zhang ZZ (2008) Constitutive model for the mechanical behaviors of bcc and fcc nanocrystalline metals over a wide strain rate range. Mater Sci Eng, A 480:419–427

[9] Ivanisenko Y, Werz T, Minkow A, Lohmiller J, Gruber PA, Kobler A, Kurmanaeva L, Fecht HJ (2013) Observation of shear band formation in nanocrystalline Pd–Au alloy during in situ SEM compression testing. J Mater Sci 48:6841–6847

[10] Cheng S, Ma E, Wang YM, Kecskes LJ, Youssef KM, Kock CC, Trociewitz UP, Han K (2005) Tensile properties of in situ consolidated nanocrystalline Cu. Acta Mater 53:1521–1533

[11] Zhu RT, Zhou JQ, Jiang H, Zhang DS (2010) Strain localization of fully dense nanocrystallie Ni sheet. J Mater Sci 45:759–764

[12] Chan T, Zhou Y, Brooks I, Palumbo G, Erb U (2014) Localized strain and heat generation during plastic deformation in nanocrystalline Ni and Ni–Fe. J Mater Sci 49:3847–3859

[13] Yoo SH, Sudarshan TS, Sethuram K (1999) Consolidation and high strain rate mechanical behavior of nanocrystalline tantalum powder. Nanostruct Mater 12:23–28

[14] Zhu RT, Zhang XX, Li YF, Zhou JQ (2013) Impact behavior and constitutive model of nanocrystalline Ni under high strain rate loading. Mater Des 49:426–432

[15] Nyakiti LO, Jankowski AF (2010) Characterization of strain rate sensitivity and grain boundary structure in nanocrystalline gold–copper alloys. Metall Mater Trans A 41:838–847

[16] Wu TW, Doerner MF, Oliver WC, Pharr GM, Brotzen FR (1990) Thin film stress and mechanical properties II. Mater Res Soc Symp Proc 188:p191

[17] Barletta M, Gisario A, Lusvarghi L, Bolelli G, Rubino G (2008) On the combined use of scratch tests and CLA profilometry for the characterization of polyester powder coating: influence of scratch load and speed. Appl Surf Sci 254:7198–7214

[18] Conrad H (2003) Grain size dependence of the plastic deformation kinetics in Cu. Mater Sci Eng A 341:216–228

[19] Asaro RJ, Suresh S (2005) Mechanistic models for the activation volume and rate sensitivity in metals with nanocrystalline grains and nano-scale twins. Acta Mater 53:3369–3382

[20] Zhou JQ, Li ZH, Zhu RT, Li YL, Zhang ZZ (2008) A mixtures-based model for the grain size dependent mechanical behavior of nanocrystalline materials. J Mater Process Tech 197:325–336